

Prompt-based Dynamic Token Pruning to Guide Transformer Attention in Efficient Segmentation

Pallabi Dutta¹, Anubhab Maity¹, and Sushmita Mitra¹

Machine Intelligence Unit, Indian Statistical Institute, Kolkata

Abstract. The high computational demands of Vision Transformers (ViTs), in processing a huge number of tokens, often constrain their practical application in analyzing medical images. This research proposes an adaptive prompt-guided pruning method to selectively reduce the processing of irrelevant tokens in the segmentation pipeline. The prompt-based spatial prior helps to rank the tokens according to their relevance. Tokens with low-relevance scores are down-weighted, ensuring that only the relevant ones are propagated for processing across subsequent stages. This data-driven pruning strategy facilitates end-to-end training, maintains gradient flow, and improves segmentation accuracy by focusing computational resources on essential regions. The proposed framework is integrated with several state-of-the-art models to facilitate the elimination of irrelevant tokens; thereby, enhancing computational efficiency while preserving segmentation accuracy. The experimental results show a reduction of $\sim 35\text{-}55\%$ tokens; thus reducing the computational costs relative to the baselines. Cost-effective medical image processing, using our framework, facilitates real-time diagnosis by expanding its applicability in resource-constrained environments.

Keywords: Box Prompt, Vision-Transformer, Pruning, Segmentation

1 Introduction

Precise segmentation of anatomical or pathological areas in medical images is important for clinical applications, such as disease diagnosis, treatment planning, surgical navigation, and personalized medicine. It allows clinicians to measure the burden of the disease, evaluate the response to treatment, and ultimately improve the patient’s outcome. Deep learning [1] has revolutionized medical image analysis by offering powerful algorithms to automate complex tasks such as segmentation. Its ability to learn intricate patterns from large datasets without much human intervention has made it a popular choice. Vision Transformers (ViTs) [2] have recently gained prominence in the development of algorithms for various computer vision tasks, including medical image segmentation.

ViTs employ self-attention mechanism to capture long-range dependencies in images, thus facilitating global context awareness. This is beneficial for segmentation of anatomical structures that exhibit diverse shapes and sizes. The global view enables ViTs to model interactions between far-apart image regions,

which can be difficult for convolutional networks with their restricted receptive fields. Several ViT-based segmentation approaches *viz.* UNETR [3], TransUNET [4], Swin-UNETR [5] and SegFormer [6] have reported encouraging performance in medical image segmentation, achieving state-of-the-art results across various benchmarks.

Despite impressive performance, ViTs face limitation in handling resource-constrained environments due to the quadratic computational complexity of self-attention. This scales poorly with increasing input image dimensions. Consequently, the deployment of ViT-based segmentation models in real-time clinical environments becomes challenging, limiting their applicability in practice.

Model compression techniques, including pruning, offer an effective way to mitigate the computational expenses associated with ViTs. Pruning reduces the computational cost of a model by removing less significant elements from its architecture. Static pruning [7,8,9] removes fixed components of the model architecture, before inference, by irreversibly eliminating components considered less significant. Although effective in minimizing model size and computational expense, static pruning is less flexible [10]. Its rigid nature limits the ability to adjust to the unique features of each input image. This constraint poses significant challenges for the analysis of medical images, where the variability between images can be considerable.

In contrast, dynamic pruning [11] adaptively adjusts the computation at inference by selectively deactivating model components based on input. Token pruning increases efficiency by reducing the number of processed tokens. Early exit strategies [12,13] save computation by bypassing the processing of specific layers for a subset of tokens. However, they might introduce representation inconsistencies within the network. The importance scores for weighting tokens in dynamic token pruning approaches [14,15,16] are often learned without explicit consideration of prior spatial knowledge about the varying target anatomical structures. This might lead to suboptimal segmentation results.

To address these limitations, we introduce a *Prompt-driven Adaptive Token Pruning* approach that explicitly incorporates structured spatial priors into the pruning process. In contrast to techniques that depend exclusively on attention scores or heuristics for selecting tokens, our method utilizes the spatial information embedded in the box prompts to direct token retention. It facilitates input-specific adaptation of the network computation. This guarantees the preservation of tokens essential for depicting the structure of the target object, while redundant or less informative tokens are removed. By directly incorporating this spatial constraint, the proposed method improves the precision of the segmentation and optimizes computational efficiency.

Section 2 provides a comprehensive overview of the steps involved in the proposed token pruning framework. The experimental results and details of implementation are presented in Section 3, in the publicly available datasets ACDC [17] and ISIC [18]. Qualitative and quantitative results derived from the application of our framework, as embedded in state-of-the-art ViT-based segmentation models, are described. Section 4 provides a summary of the concluding remarks.

2 Methodology

This section details our proposed Prompt-Driven Token Pruning framework, in the context of the architecture of prevalent segmentation networks, as well as the token generation mechanism adopted in ViTs. Recent high-performance medical image segmentation models employ an U -shaped encoder-decoder architecture [19]. ViT-based models typically employ ViT blocks either at the bottleneck of the encoder-decoder structure or throughout the entire encoder path. This study focuses on architectures associated with both frameworks.

2.1 Token generation in ViT

ViTs transform an input image (or feature map volume) $I \in \mathbb{R}^{C \times H \times W}$ into a sequence of tokens [2]. Here, H , W and C represent the height, width, and channel dimensions of I . The input is partitioned into a set of non-overlapping patches Z ; $|Z| = \frac{HW}{p^2}$, with each patch having dimension p^2 . They are flattened and linearly projected in C' -dimensional embedding space, resulting in the sequence $P' \in \mathbb{R}^{Z \times C'}$. These embedded vectors are called tokens. Positional embedding is added to the tokens to retain their spatial locations. $P_0 \in \mathbb{R}^{Z \times C'}$ is the sequence of position-sensitive tokens that serve as input to a transformer encoder.

This encoder block consists of alternating layers of multi-head self-attention (μ) and feed-forward network (Φ) units. The μ captures global contextual relationships between different tokens, performing self-attention parallelly across multiple heads, to operate in various representational subspaces. Φ is independently applied to the output of each head, to enhance their representational capacity by including an additional non-linear transformation. The operations within a transformer block are expressed as $Y_{out} = \Phi(LN(Y)) + \mu(LN(P_0)) + P_0$, where LN [20] is the Layer Normalization and $Y_{out} \in \mathbb{R}^{Z \times C'}$ is the final output of the transformer block.

2.2 Prompt-driven adaptive pruning

Prompts serve as a prior by offering high-level, task-specific information. This directs the model to focus on segmenting specific structures within the input image, resulting in effective segmentation. Consequently, it allows token selection based on contextual information. This framework is referred to as *prompt-driven adaptive pruning*, where essential tokens are preserved while down-weighting the irrelevant ones to minimize their processing.

Score map compute: At a given stage l , employing a ViT block, the output tokens Y_{out} are combined with box-prompt coordinates $(x_{min}, y_{min}), (x_{max}, y_{max})$ to extract region-specific features $F \in \mathbb{R}^{k \times k \times C'}$ from the area defined by the prompt using RoIAlign [21]. The box prompts serve as spatial priors, guiding the selection of relevant features by focusing on the most informative regions. This facilitates the extraction of region-specific feature embeddings corresponding to the Region-of-Interest (RoI) defined in the prompt.

In addition, a similarity score map $S \in \mathbb{R}^{M \times Z}$ is calculated between the region-specific feature, encoded by F and Y_{out} , to measure the relevance of each token. The F and Y_{out} are first transformed into lower-dimensional embeddings $V_1 \in \mathbb{R}^{M \times d_V}$ and $V_2 \in \mathbb{R}^{Z \times d_V}$, respectively, with projection matrices $f_1 \in \mathbb{R}^{C' \times d_V}$ and $f_2 \in \mathbb{R}^{C' \times d_V}$. This reduces computational complexity while improving feature discrimination. M denotes the number of feature vectors in V_1 . The similarity score is computed as

$$S(V_1, V_2) = V_1 V_2^T / \sqrt{d_V}; V_1 = f_1 \cdot F; V_2 = f_2 \cdot Y_{out}. \quad (1)$$

Prune mask compute: Here S is normalized along the token dimension to generate a probability distribution $\rho \in \mathbb{R}^{M \times Z}$. The probability ρ_{ij} of the i th feature vector of V_1 (V_{1i}) that it is relevant to the j th feature vector of V_2 (V_{2j}) is given as $\rho_{ij} = \frac{e^{(S_{ij})}}{\sum_{k=1}^Z e^{S_{ik}}}$. S_{ij} denotes the similarity score between V_{1i} and V_{2j} . Next, the Shannon entropy [22] $H(\cdot)$ is calculated for the probability distribution of each V_{1i} , over all the ViT tokens. This yields

$$H(V_{1i}) = - \sum_{j=1}^Z \rho_{ij} \log(\rho_{ij}), \quad (2)$$

with $H(V_{1i})$ quantifying the uncertainty of association between V_{1i} and the set of all ViT tokens. A lower value of $H(V_{1i})$ implies a strong association with a subset of tokens. Conversely, a higher value indicates that V_{1i} is uncertain about its association with the tokens.

An inverse entropy weighting scheme is applied to prioritize tokens having lower uncertainty values. The entropy values are first ranked in ascending order. The ranks $R_i | i \in [1, M]$ are normalized to ensure their uniform spacing between 0 and 1. Inverse entropy weights $\Omega_i = 1 - R_i$, with $\Omega = \{\Omega_i | i \in [1, M]\}$, ensure that higher entropy values (more uncertainty) are assigned to the lower weights and vice versa.

Lemma 1 (Uniformity of Weights). *If the normalized ranks R_i are uniformly distributed on $[0, 1]$, then the transformed weights Ω are also uniformly distributed over $[0, 1]$. In other words, applying the transformation $\Omega_i = 1 - R_i$ preserves the uniformity of the distribution, merely reversing the order of values.*

Proof. Since $R_i \sim \text{Uniform}(0, 1)$, its cumulative distribution function (CDF) is

$$F_R(x) = P(R_i \leq x) = x, \quad x \in [0, 1].$$

For the transformed weights $\Omega_i = 1 - R_i$, the CDF becomes

$$F_\Omega(x) = P(\Omega_i \leq x) = P(1 - R_i \leq x) = P(R_i \geq 1 - x).$$

Since $R_i \sim \text{Uniform}(0, 1)$, we substitute its CDF as

$$P(R_i \geq 1 - x) = 1 - P(R_i \leq 1 - x) = 1 - (1 - x) = x.$$

Table 1: Ablation study of UNETR on ACDC dataset, over various threshold τ .

$\tau =$	0.3	0.5	Percentile		
			25 th	50 th	75 th
GFLOPs	13.32	9.07	26.78	37.31	18.66
mDSC	0.670 \pm 0.07	0.661 \pm 0.09	0.693 \pm 0.07	0.695 \pm 0.08	0.657 \pm 0.09

Thus,

$$F_{\Omega}(x) = x, \quad x \in [0, 1].$$

Since this matches the CDF of a uniform distribution over $[0, 1]$, we conclude that $\Omega_i \sim \text{Uniform}(0, 1)$. \square

The weighted similarity score map becomes $\tilde{S} = S.\Omega$, with the overall relevance r_i of the i th token being the mean of the weighted similarity scores

$$r_i = \frac{1}{C'} \sum_{j=1}^{C'} \tilde{S}_{ij}. \quad (3)$$

The final step modifies the original tokens, based on their relevance scores. A binary mask $\beta \in \{0, 1\}^Z$ is generated by applying a threshold τ on the relevance scores as

$$\beta_i = \begin{cases} 1, & \text{if } \sigma(r_i) > \tau, \\ 0, & \text{otherwise.} \end{cases} \quad (4)$$

Here σ is the sigmoid function to squash the relevance scores to range $[0, 1]$, and β is applied to ViT tokens Y_{out} for effectively removing tokens that are deemed irrelevant based on our proposed prompt-guided weighting and thresholding. The masked token Y'_{out} is generated by element-wise multiplication (\odot) of β with Y_{out} , *i.e.* $Y'_{out} = \beta \odot Y_{out}$.

3 Experimental Results

The proposed framework is evaluated on state-of-the-art ViT-based segmentation models, *viz.* UNETR, TransUNET, SegFormer and Swin UNETR. The Dice Score Coefficient (*DSC*) is used to compare the segmentation performance between the original baselines and their adaptations after incorporating our prompt-based token pruning. The evaluation is performed on publicly available ACDC [17] and ISIC [18] datasets. ACDC comprises 150 chest MRI images with ground truth delineations for right ventricle, left ventricle and myocardium. ISIC contains 2000 dermoscopic images with corresponding pixel-level annotations for skin lesions. The adopted train-test-validation split is 80:10:10. The models were trained in Python 3.9, using PyTorch and MONAI libraries, on NVIDIA RTX A5500 GPU with 24GB of memory.

Table 2: Ablation study of UNETR on ACDC dataset, with pruning performed at different stages.

Stage #	{1}	{1,2}	{1,2,3}	{1,2,3,4}	Baseline
GFLOPs	37.42	26.78	37.35	37.31	37.46
mDSC	0.673 ± 0.08	0.693 ± 0.07	0.687 ± 0.08	0.692 ± 0.08	0.669 ± 0.08

Table 3: Ablation study, in terms of mean DSC and standard deviation across all test samples, incorporating *prompt-based adaptive pruning* framework on different baseline models.

Models \ Datasets	ACDC						ISIC	
	Ventricle				Myocardium		Base	Pruned
	Left		Right		Base	Pruned		
UNETR	0.552 ± 0.016	0.594 ± 0.001	0.695 ± 0.009	0.720 ± 0.017	0.777 ± 0.006	0.782 ± 0.005	0.833 ± 0.009	0.875 ± 0.013
Swin UNETR	0.64 ± 0.009	0.662 ± 0.018	0.794 ± 0.018	0.785 ± 0.006	0.846 ± 0.011	0.854 ± 0.017	0.885 ± 0.015	0.883 ± 0.007
TransUNET	0.640 ± 0.011	0.706 ± 0.007	0.769 ± 0.008	0.831 ± 0.005	0.871 ± 0.005	0.882 ± 0.009	0.824 ± 0.011	0.825 ± 0.018
SegFormer	0.684 ± 0.011	0.679 ± 0.013	0.822 ± 0.015	0.816 ± 0.011	0.898 ± 0.019	0.902 ± 0.004	0.812 ± 0.008	0.822 ± 0.002

Table 1 quantifies the experimental results of fixed threshold values (0.3, 0.5) and adaptive percentile-based threshold values (25^{th} , 50^{th} , 75^{th}) for τ . Increasing the fixed value of τ from 0.3 to 0.5 reduces the computational cost. However, it may lead to over-pruning of relevant tokens due to a decrease in the mean DSC value. Lower percentile values (25^{th} and 50^{th}) retain comparatively more tokens than higher percentiles (75^{th}), as indicated by the increase in Giga Floating Point Operations (GFLOPs). τ at the 25^{th} percentile is found to have the optimal balance between accuracy and computational efficiency. Discarding 75% of the total tokens results in suboptimal segmentation performance due to information loss. Adaptive percentile-based thresholding provides greater flexibility to the token pruning mechanism than fixed threshold values, and achieves a superior balance between segmentation performance and computational costs.

Table 2 presents the results of the application of the proposed token pruning framework in multiple stages of UNETR. Pruning tokens at levels 1 and 2 drastically reduces the computational cost by 28%, with an associated increase in the mean value of DSC by 3%. Applying pruning to deeper levels of the network leads to a saturated segmentation performance without a significant decrease in computational efficiency. Therefore, early-stage pruning effectively removes irrelevant tokens and prevents them from spreading deeper into the network.

Table 3 summarizes the values of DSC for different baselines, as well as their pruned versions, in the ACDC and ISIC datasets. UNETR and TransUNET exhibit significant performance gains (1% – 7% approx.) in DSC values in both datasets. This suggests that the prompt-based spatial prior helps the model focus more on relevant regions. Swin UNETR and SegFormer demonstrate stable performance, even after substantial token removal, as seen in Fig. 1. Therefore, the proposed framework improves the overall segmentation accuracy by retaining relevant tokens for target structures.

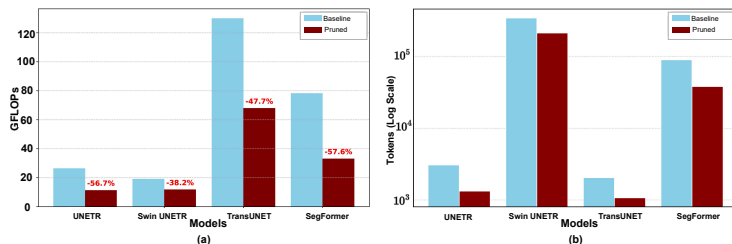


Fig. 1: Graphical plot, comparing (a) GFLOPs and (b) Token Sparsity of the baselines w.r.t. their pruned versions.

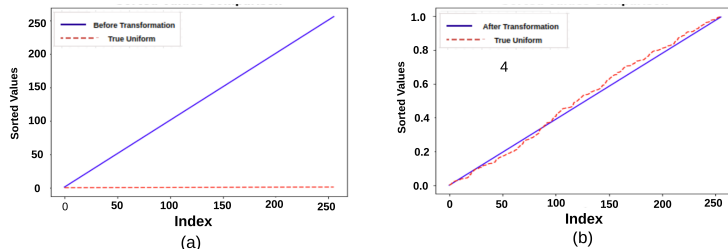


Fig. 2: Line plots comparing the (a) non-uniform distribution of token relevance ranking, and (b) uniform distribution of entropy-based weighting, for an image.

Fig. 1(a) illustrates that the proposed framework significantly reduces computational costs across all models. The pruned variants of SegFormer and UNETR show the highest reduction in terms of GFLOPs. Fig. 1(b) depicts a significant decrease in the token density of the pruned variants, compared to their respective baselines. This elimination of irrelevant tokens leads to computationally efficient segmentation models. Fig. 2 demonstrates that the token relevance ranking distribution is naturally non-uniform, capturing differences in importance. The entropy-based weighting, on the other hand, is uniformly distributed. This is consistent with the theoretical analysis of the proposed approach, and confirms its efficacy in pruning.

Fig. 3 shows the token retention maps, generated for a sample input image, by the pruned version of the baselines. The variation in the percentage of pruned tokens for the same sample, across all models, highlights the specific feature learning mechanism of the different models. Swin UNETR, employing window-based self-attention, is found to retain the highest number of tokens. On the contrary, models utilizing full self-attention mechanisms like SegFormer exhibit comparatively higher token redundancy; as is evident from the lower percentage of tokens retained. The spread-out nature of the retained tokens implies that the model still retains global contextual information to some extent. This is necessary for efficient segmentation.

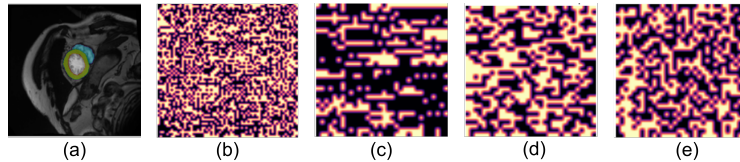


Fig. 3: (a) Sample input slice from ACDC, with token retention maps using (b) Swin UNETR, (c) SegFormer, (d) UNETR, and (e) TransUNET.

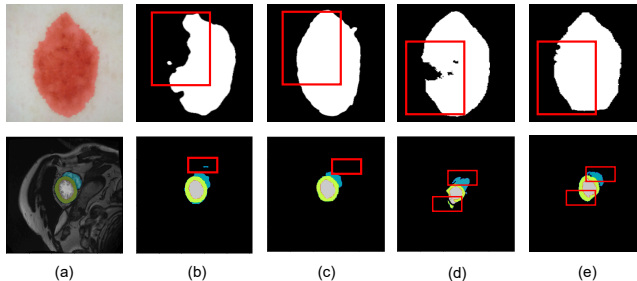


Fig. 4: Qualitative results on sample images, illustrating (a) input image, with overlaid ground truth and prediction from (b) SegFormer (baseline), (c) SegFormer (pruned), (d) UNETR (baseline), and (e) UNETR (pruned). Row 1: ISIC, Row 2: ACDC, sample images. Red boxes denote comparison area.

Fig. 4 qualitatively analyses the effectiveness of the proposed framework. The samples highlight cases where the pruned version effectively addresses issues of over- and under-segmentation in prediction by the baselines.

4 Conclusions and Discussion

This study introduces an adaptive framework for token pruning in Vision Transformers (ViT), designed to decrease the computational resources required to process irrelevant tokens. Using spatial priors through box prompts enhances the retention of semantically relevant tokens related to the target anatomical structure, thus improving segmentation accuracy. The calculation of the entropy-guided similarity score, to identify tokens aligned with the spatial prior, ensures that the token selection process is data-driven. This allows robustness to variations within the different input images. The experimental results suggest that the framework reduces the computational cost while maintaining (or even improving) the segmentation performance in certain scenarios. This study can be further extended to other transformer-based segmentation models and incorporate multiple types of prompts to gain additional insight into the generalizability of the proposed pruning approach.

References

1. Y. LeCun, Y. Bengio, and *et al.*, “Deep learning,” *Nature*, vol. 521, pp. 436–444, 2015.
2. A. Dosovitskiy, “An image is worth 16x16 words: Transformers for image recognition at scale,” *arXiv preprint arXiv:2010.11929*, 2020.
3. A. Hatamizadeh, Y. Tang, and *et al.*, “UNETR: Transformers for 3D medical image segmentation,” in *Proceedings of the IEEE/CVF Winter Conference on Applications of Computer Vision*, pp. 574–584, 2022.
4. J. Chen, Y. Lu, and *et al.*, “TransUNet: Transformers make strong encoders for medical image segmentation,” *arXiv preprint arXiv:2102.04306*, 2021.
5. A. Hatamizadeh, V. Nath, and *et al.*, “Swin UNETR: Swin transformers for semantic segmentation of brain tumors in MRI images,” in *Proceedings of the International MICCAI BrainLesion Workshop*, pp. 272–284, Springer, 2021.
6. E. Xie, W. Wang, Z. Yu, and *et al.*, “SegFormer: Simple and efficient design for semantic segmentation with transformers,” *Advances in Neural Information Processing Systems*, vol. 34, pp. 12077–12090, 2021.
7. C. I. López-González, E. Gascó, and *et al.*, “Filter pruning for convolutional neural networks in semantic image segmentation,” *Neural Networks*, vol. 169, pp. 713–732, 2024.
8. C. Sun, J. Chen, and *et al.*, “Channel pruning method driven by similarity of feature extraction capability,” *Soft Computing*, pp. 1–20, 2025.
9. M. Adnan, Q. Ba, and *et al.*, “Structured model pruning for efficient inference in computational pathology,” in *International workshop on Medical Optical imaging and Virtual microscopy Image analysis (MOVI)*, pp. 140–149, Springer, 2024.
10. Y. He and L. Xiao, “Structured pruning for deep convolutional neural networks: A survey,” *IEEE Transactions on Pattern Analysis and Machine Intelligence*, vol. 46, pp. 2900–2919, 2023.
11. S. Liu, L. Wang, and W. Yue, “An efficient medical image classification network based on multi-branch CNN, token grouping transformer and mixer MLP,” *Applied Soft Computing*, vol. 153, p. 111323, 2024.
12. Q. Tang, B. Zhang, and *et al.*, “Dynamic token pruning in plain vision transformers for semantic segmentation,” in *Proceedings of the IEEE/CVF International Conference on Computer Vision*, pp. 777–786, 2023.
13. Y. Tian, L. Xie, and *et al.*, “Beyond masking: Demystifying token-based pre-training for Vision Transformers,” *Pattern Recognition*, vol. 162, p. 111386, 2025.
14. Y. Rao, W. Zhao, and *et al.*, “DynamicViT: Efficient Vision Transformers with Dynamic Token Sparsification,” *Advances in Neural Information Processing Systems*, vol. 34, pp. 13937–13949, 2021.
15. X. Lin, L. Yu, and *et al.*, “The lighter the better: Rethinking transformers in medical image segmentation through adaptive pruning,” *IEEE Transactions on Medical Imaging*, vol. 42, pp. 2325–2337, 2023.
16. A. A. Salam, M. Z. Asaf, and *et al.*, “Skin whole slide image segmentation using lightweight-pruned transformer,” *Biomedical Signal Processing and Control*, vol. 106, p. 107624, 2025.
17. O. Bernard, A. Lalande, and *et al.*, “Deep learning techniques for automatic MRI cardiac multi-structures segmentation and diagnosis: Is the problem solved?,” *IEEE Transactions on Medical Imaging*, vol. 37, pp. 2514–2525, 2018.
18. N. C. Codella, D. Gutman, and *et al.*, “Skin lesion analysis toward melanoma detection,” in *Proceedings of the IEEE 15th International Symposium on Biomedical Imaging (ISBI)*, pp. 168–172, IEEE, 2018.

19. O. Ronneberger, P. Fischer, and *et al.*, “U-Net: Convolutional networks for biomedical image segmentation,” in *Proceedings of the International Conference on Medical Image Computing and Computer Assisted Intervention, (MICCAI)*, pp. 234–241, Springer, 2015.
20. J. Lei Ba, J. R. Kiros, and *et al.*, “Layer normalization,” *ArXiv e-prints*, pp. arXiv–1607, 2016.
21. K. He, G. Gkioxari, and *et al.*, “Mask R-CNN,” in *Proceedings of the IEEE International Conference on Computer Vision (ICCV)*, pp. 2961–2969, 2017.
22. C. E. Shannon, “A mathematical theory of communication,” *The Bell System Technical Journal*, vol. 27, pp. 379–423, 1948.